Supporting information:

Formation kinetics and mechanism of ozone and secondary organic aerosols from photochemical oxidation of different aromatic hydrocarbons: dependence of NO_x and organic substituent

Hao Luo [a,b,★], Jiangyao Chen [a,b,★], Guiying Li [a,b], Taicheng An [a,b,*]

[a] *Guangdong Key Laboratory of Environmental Catalysis and Health Risk Control, Guangdong-Hong Kong-Macao Joint Laboratory for Contaminants Exposure and Health, Institute of Environmental Health and Pollution control, Guangdong University of Technology, Guangzhou 510006, China;*

[b] *Guangzhou Key Laboratory of Environmental Catalysis and Pollution Control, Key Laboratory of City Cluster Environmental Safety and Green Development, School of Environmental Science and Engineering, Guangdong University of Technology, Guangzhou 510006, China.*

★ These authors contributed equally to this work.

*** Corresponding author:** Prof. Taicheng An, Email: antc99@gdut.edu.cn

1 Experimental setting of instrument

The gas in the reactor were inhaled into the drift tube of Proton Transfer Reaction-Time of Flight-Mass Spectrometry (PTR-ToF-MS, Ionicon Analytik, Austria) through a 1.5 m long heated PEEK tube (80 ℃) with a flow rate of 30 ml min^{-1}. The key factors of the drift tube conditions were set as following: drift pressure of 2.3 mbar, 80 ℃ and voltage at 600 V, corresponding to E/N ratio approximately 130 Td (1 Td=10^{-17} V cm^2). The PTR-TOF-MS was operated using protonated water (H_3O^+) as the reagent ion.

2 Calculation methodology

The yield of products can be calculated by the following formula:

$$\gamma_{(product)} = \triangle_{(product)} / \triangle_{(AH)} \qquad (S1)$$

which γ is the yield of a single AH product; $\triangle_{(product)}$ is the concentration of individual AH product when peak O_3 concentration occurs; $\triangle_{(AH)}$ is the reaction amount of AH when O_3 peak occurs during the experiment.

All experiments were conducted under UV light without aerosol seeds. And the aerosol particles were corrected by the wall loss. The yield calculation formula of SOA is shown as following:

$$\gamma_{(SOA)} = \triangle_{(particle\ mass\ concentration)} / \triangle_{(AH)} \qquad (S2)$$

γ (SOA) is the yield of SOA; $\triangle_{(particle\ mass\ concentration)}$ is the corrected particle mass concentration after peak O_3 concentration; $\triangle_{(AH)}$ is the reaction amount of the AH after peak O_3 concentration.

In two-product semi-empirical model, the SOA yield is defined as the ratio of produced aerosols to reacted AHs [1]:

$$\gamma_{(SOA)}=\Sigma_i\gamma_{i(SOA)} =M_0\Sigma_i (\alpha_i K_{om,i} /(1 + K_{om,i}M_0)) \quad (S3)$$

$\gamma_{(SOA)}$ is the yield of SOA, M_0 is the total mass concentration of organic matter, α_i and $K_{om,i}$ are the stoichiometric coefficient and the partition coefficient of species i.

In this model, these two products represent a class of low vapor pressure compounds and a class of high vapor pressure compounds, respectively. The two-product empirical model divides SOA into high-volatility and low-volatility, where α_i and $K_{om,i}$ are the fitting parameters and are determined by the minimum sum of squares of the residuals. SOA mass concentration is calculated by the volume concentration of SOA measured by SMPS. According to previous studies, the aerosol density of aromatic hydrocarbons ranges from 1.24 to 1.51 g cm^{-3} [2-4]. In this study, the aerosol density of aromatic hydrocarbons is selected as 1.4 g cm^{-3} to calculate the mass concentrations of SOA produced from AH-NO_x photooxidation in the peak O_3 time. All SMPS data were obtained after wall loss correction.

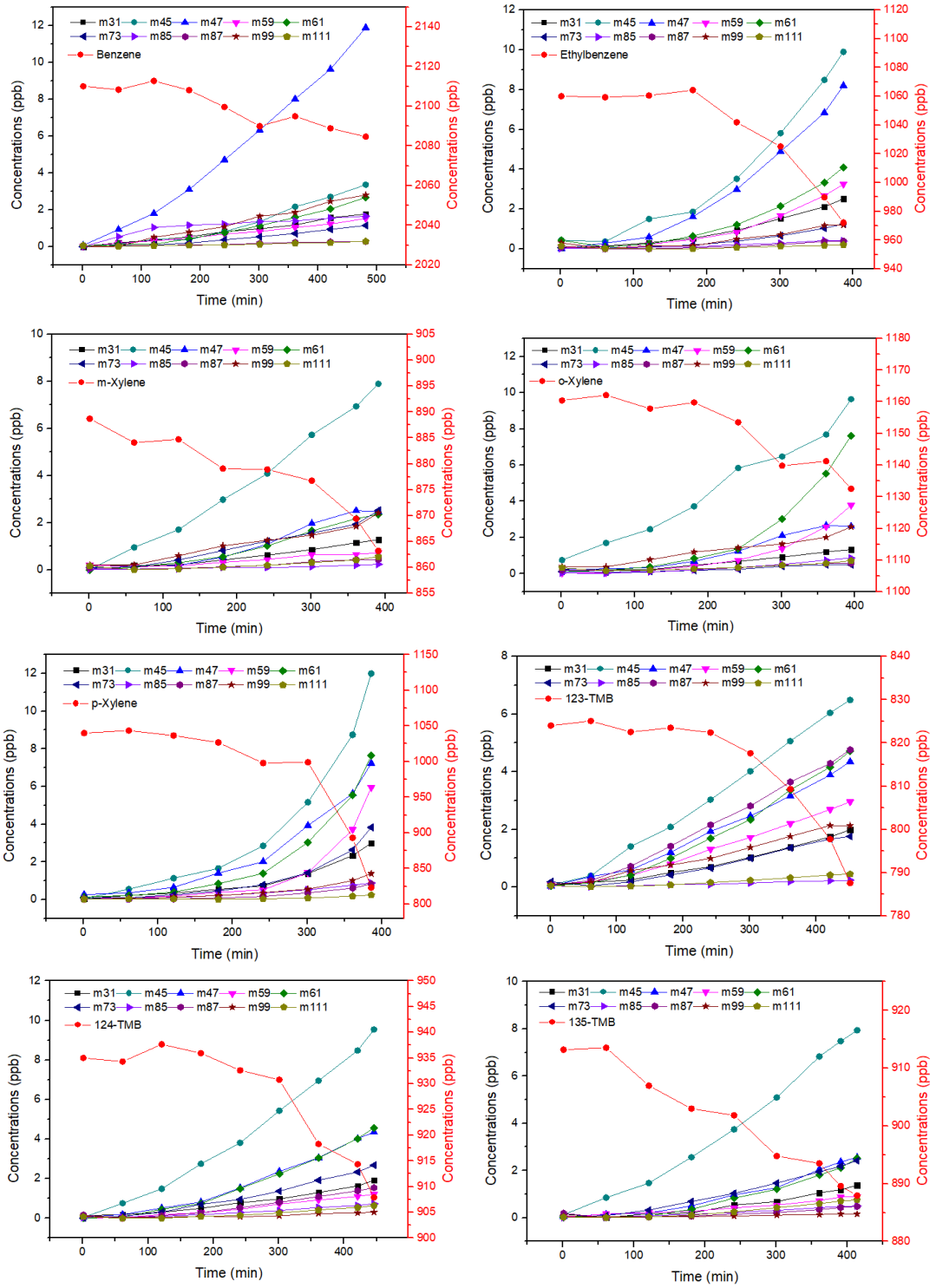

Figure S1. The concentration variation of intermediates formed from photochemical oxidation of benzene (2110 ppb), ethylbenzene (1060 ppb), m-xylene (889 ppb), o-xylene (1160 ppb), p-xylene (1040 ppb), 123TMB (824 ppb), 124TMB (935 ppb) and 135TMB (913 ppb).

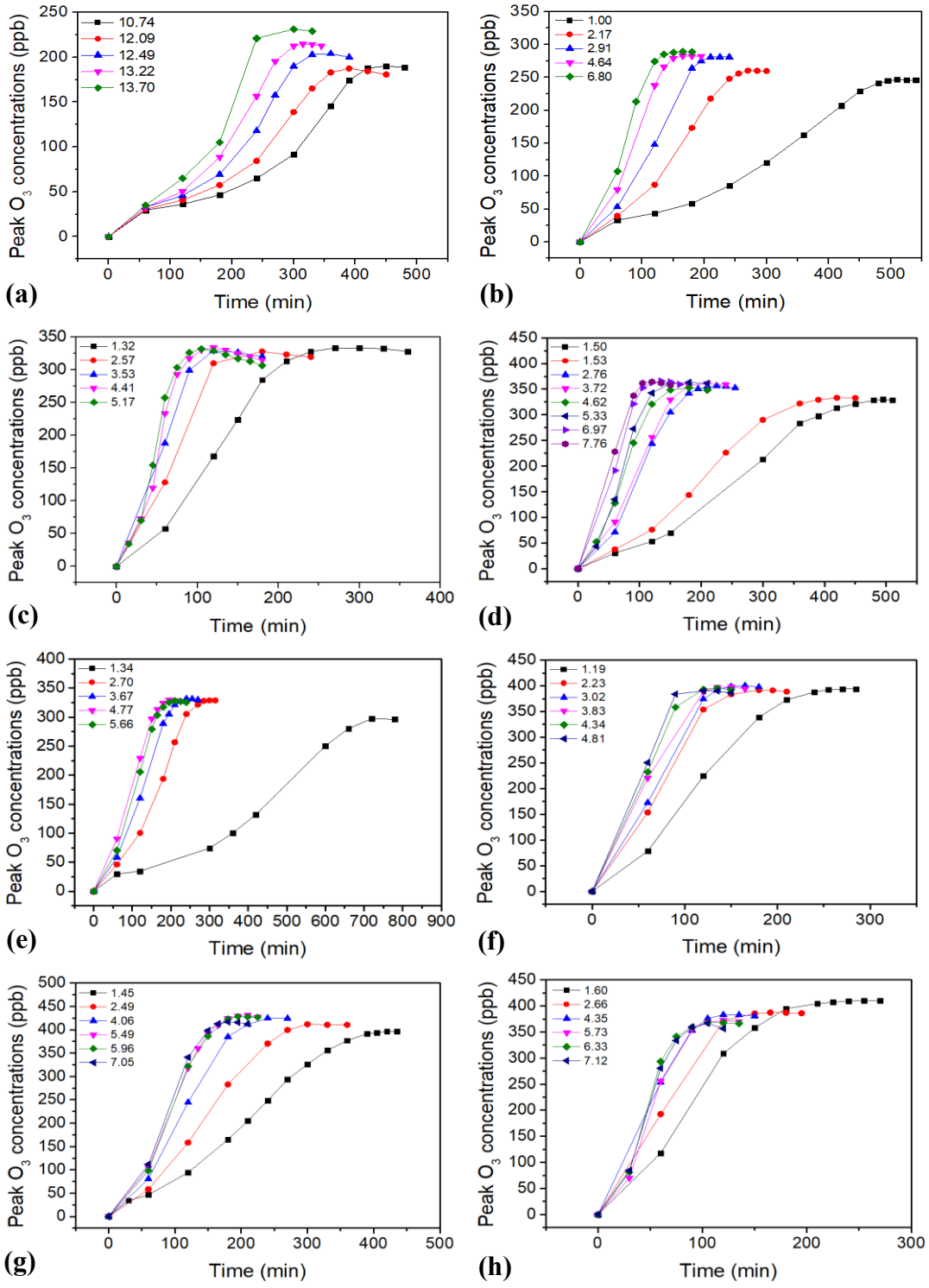

Figure S2. O_3 formation curve of benzene (a), ethylbenzene (b), m-xylene (c), o-xylene (d), p-xylene (e), 123TMB (f), 124TMB (g) and 135TMB (h) photochemical oxidation under different VOC/NO_x ratio.

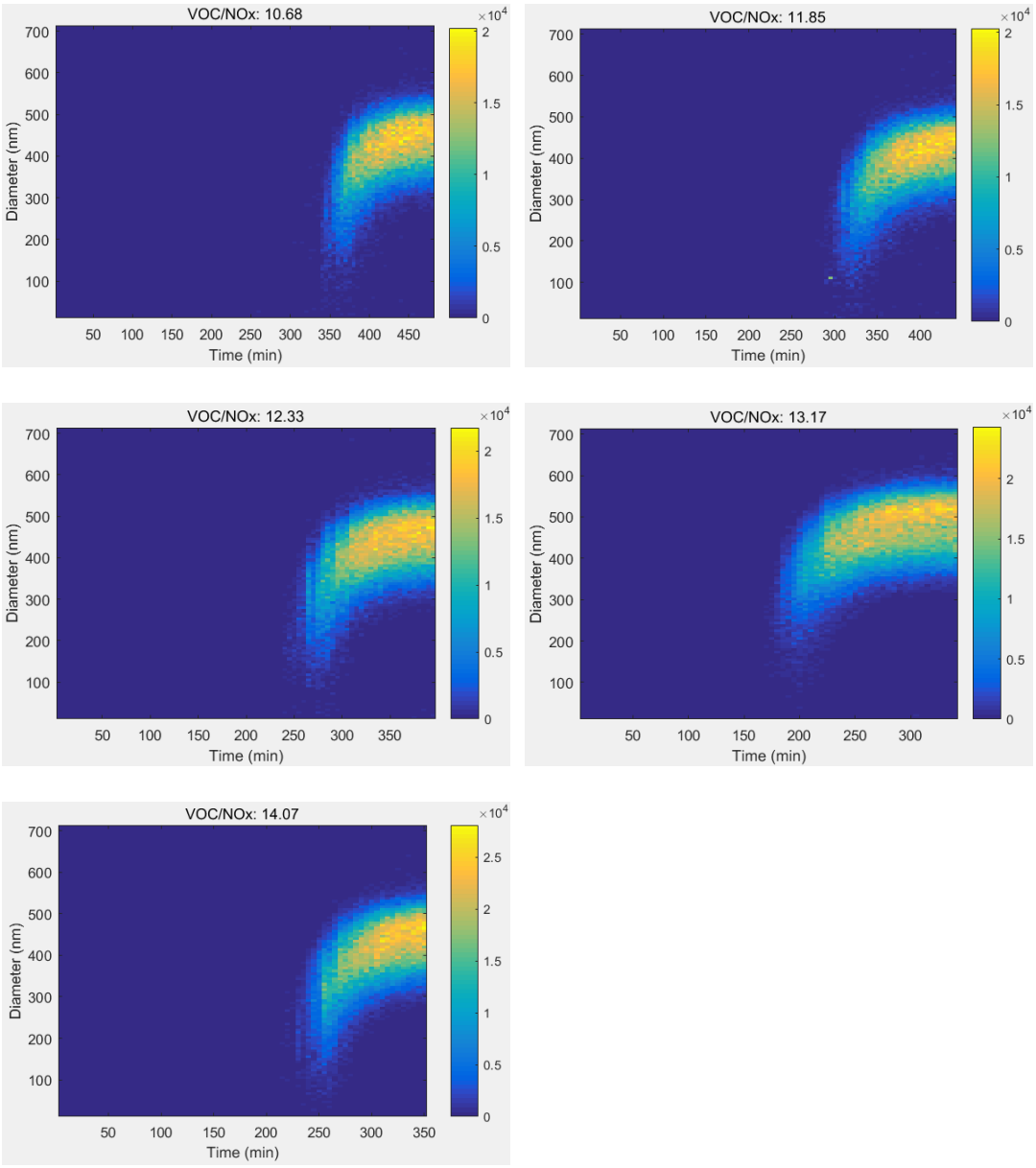

Figure S3. Nanoparticle distribution from benzene photochemical oxidation varied with time at different VOC/NO_x ratio (the initial concentrations of NO_x were in the range of 151.5 to 165.7 ppb).

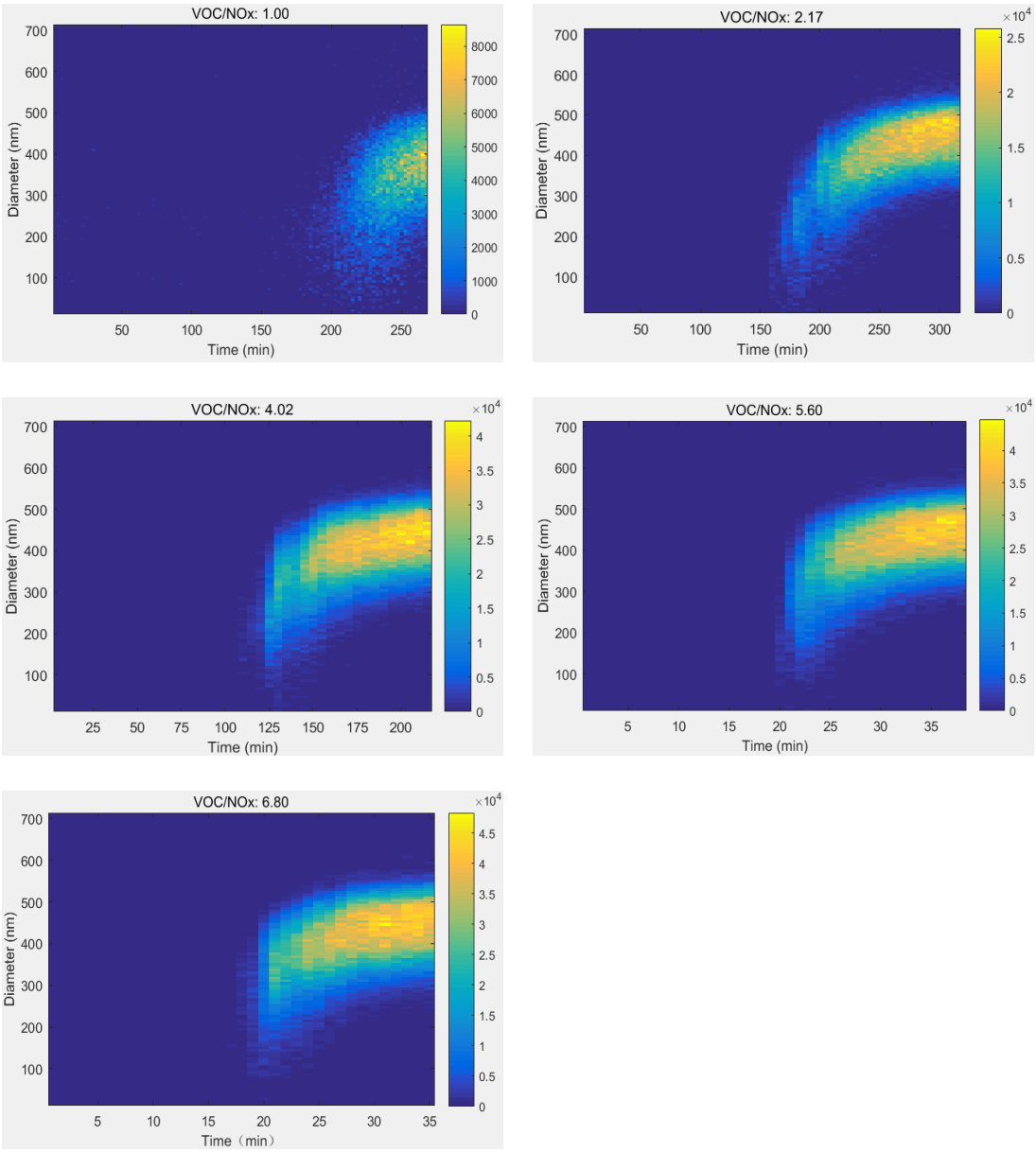

Figure S4. Nanoparticle distribution from ethylbenzene photochemical oxidation varied with time at different VOC/NO_x ratio (the initial concentrations of NO_x were in the range of 151.1 to 176.6 ppb).

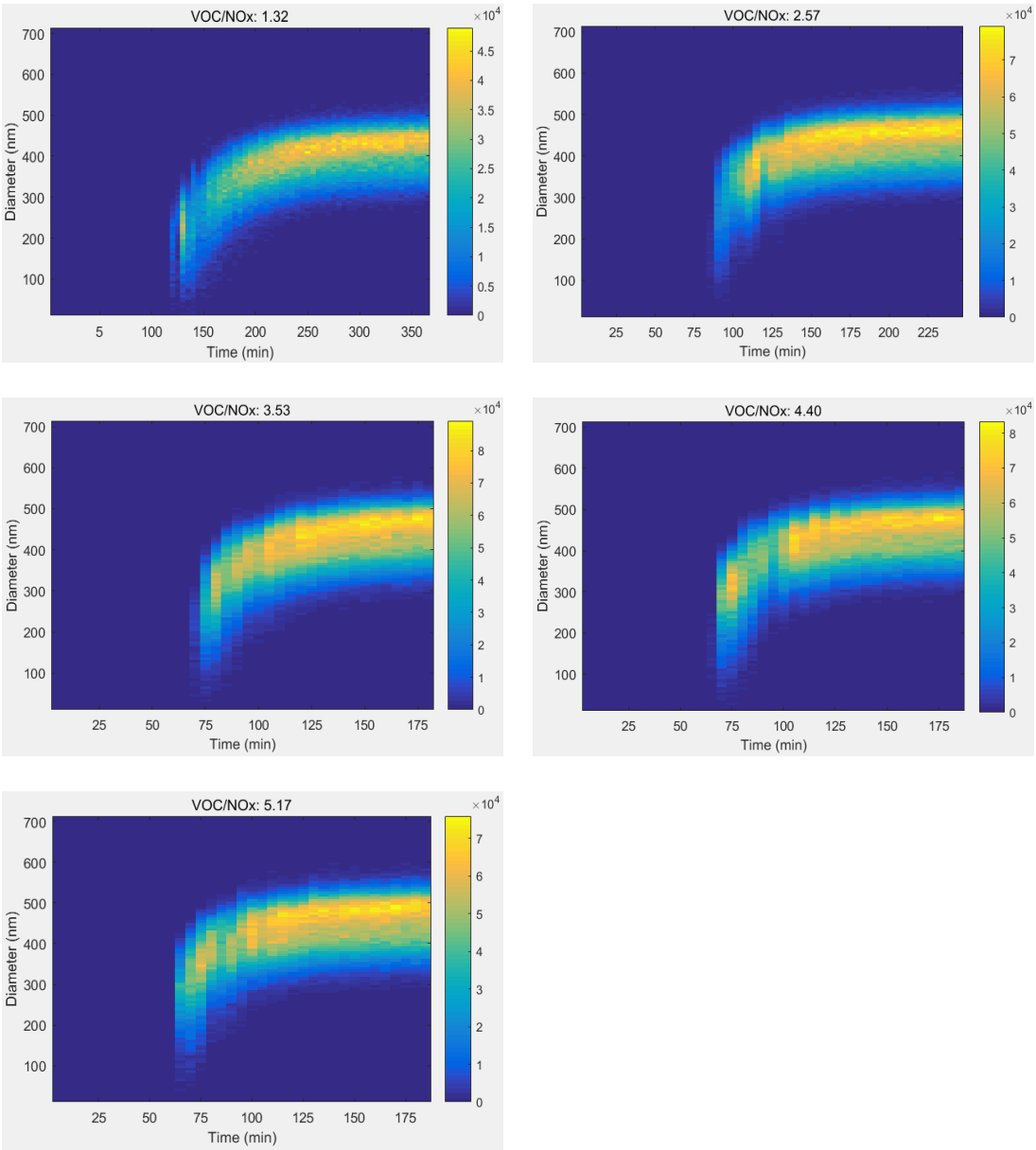

Figure S5. Nanoparticle distribution from m-xylene photooxidation varied with time at different VOC/NO_x ratio (the initial concentrations of NO_x were in the range of 169.7 to 173.6 ppb).

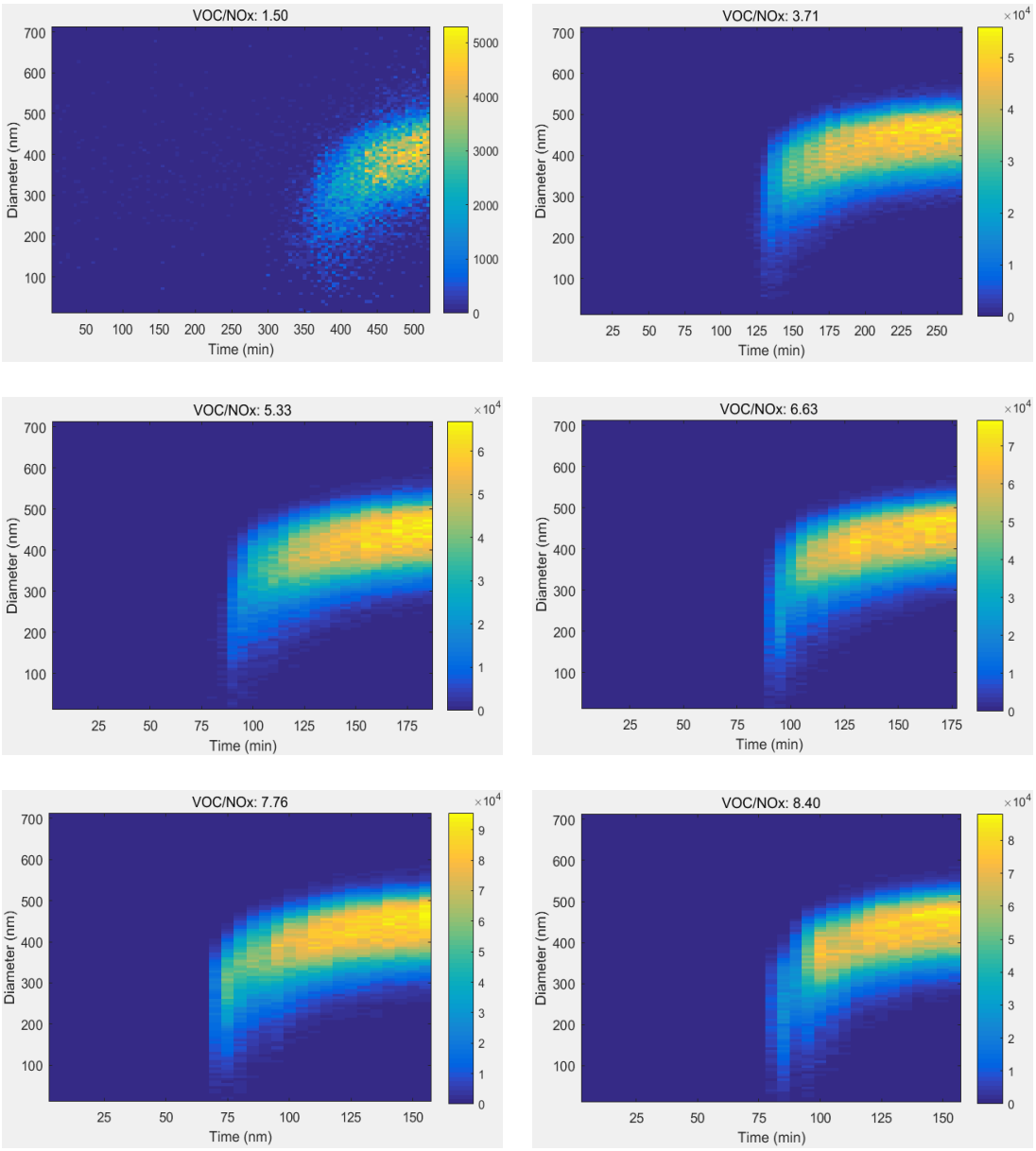

Figure S6. Nanoparticle distribution from o-xylene photooxidation varied with time at different VOC/NO_x ratio (the initial concentrations of NO_x were in the range of 157.1 to 166.4 ppb).

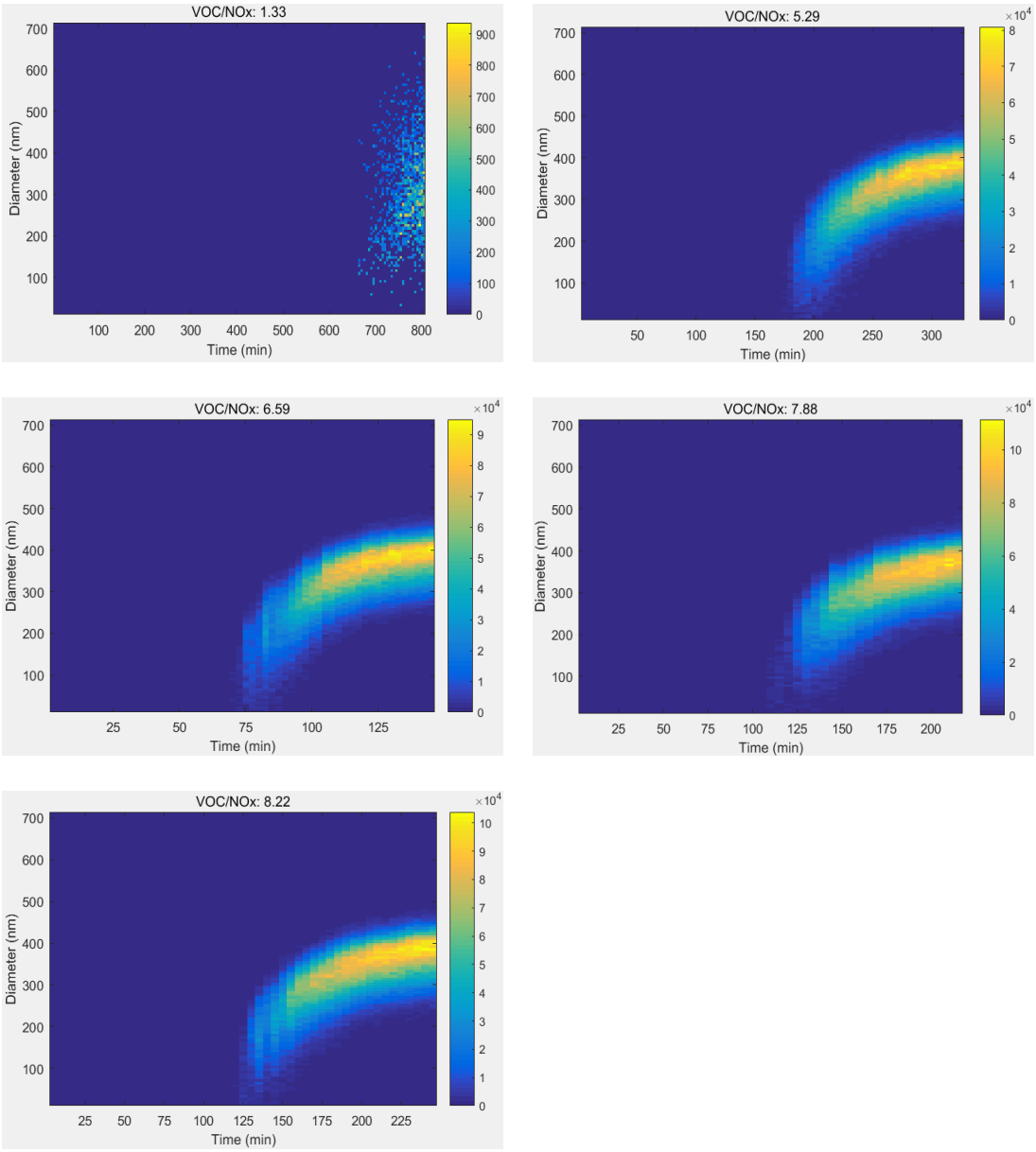

Figure S7. Nanoparticle distribution from p-xylene photooxidation varied with time at different VOC/NO_x ratio (the initial concentrations of NO_x were in the range of 157.2 to 166.9 ppb).

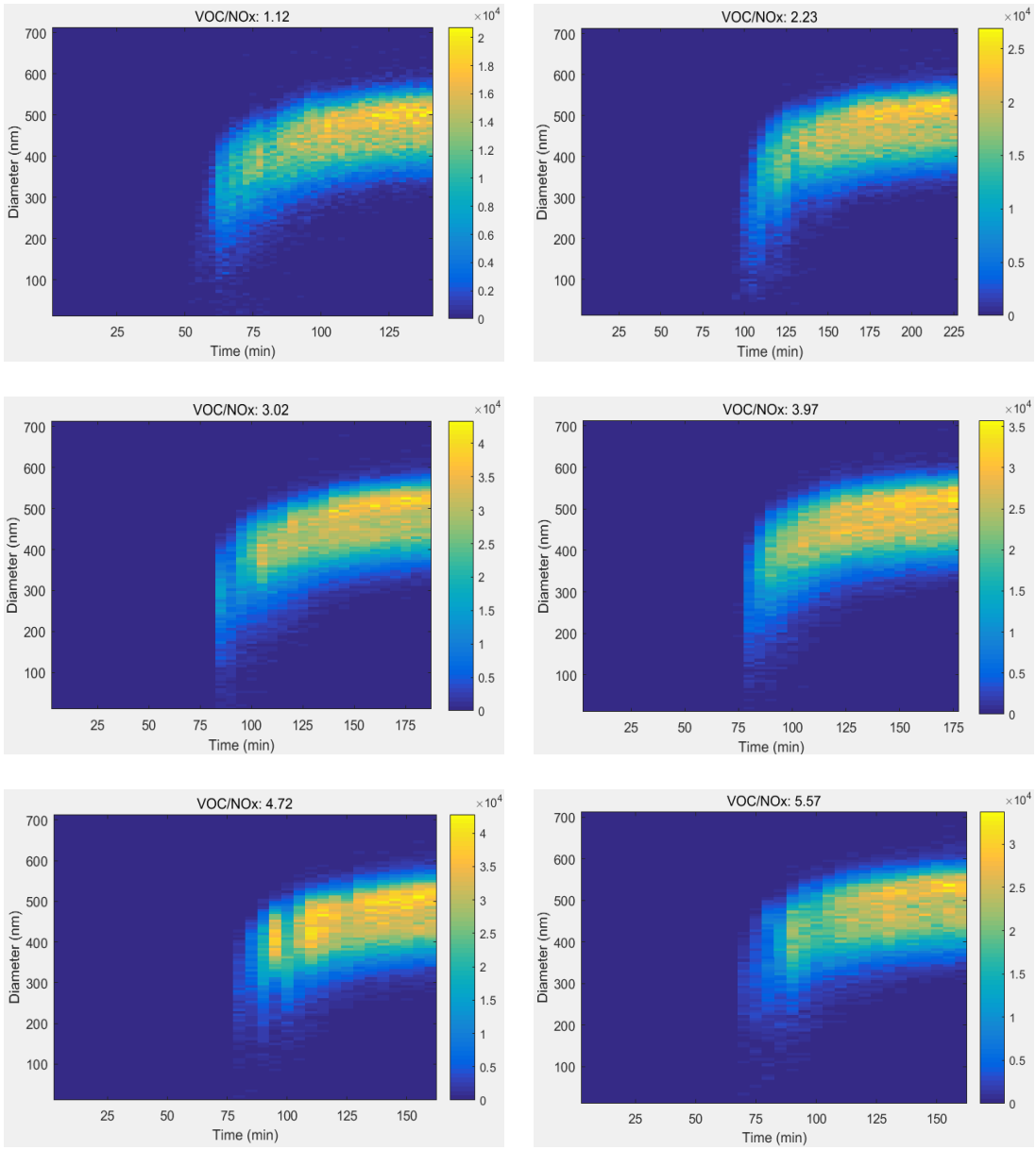

Figure S8. Nanoparticle distribution from 123TMB photooxidation varied with time at different VOC/NO_x ratio (the initial concentrations of NO_x were in the range of 167.3 to 178.4 ppb).

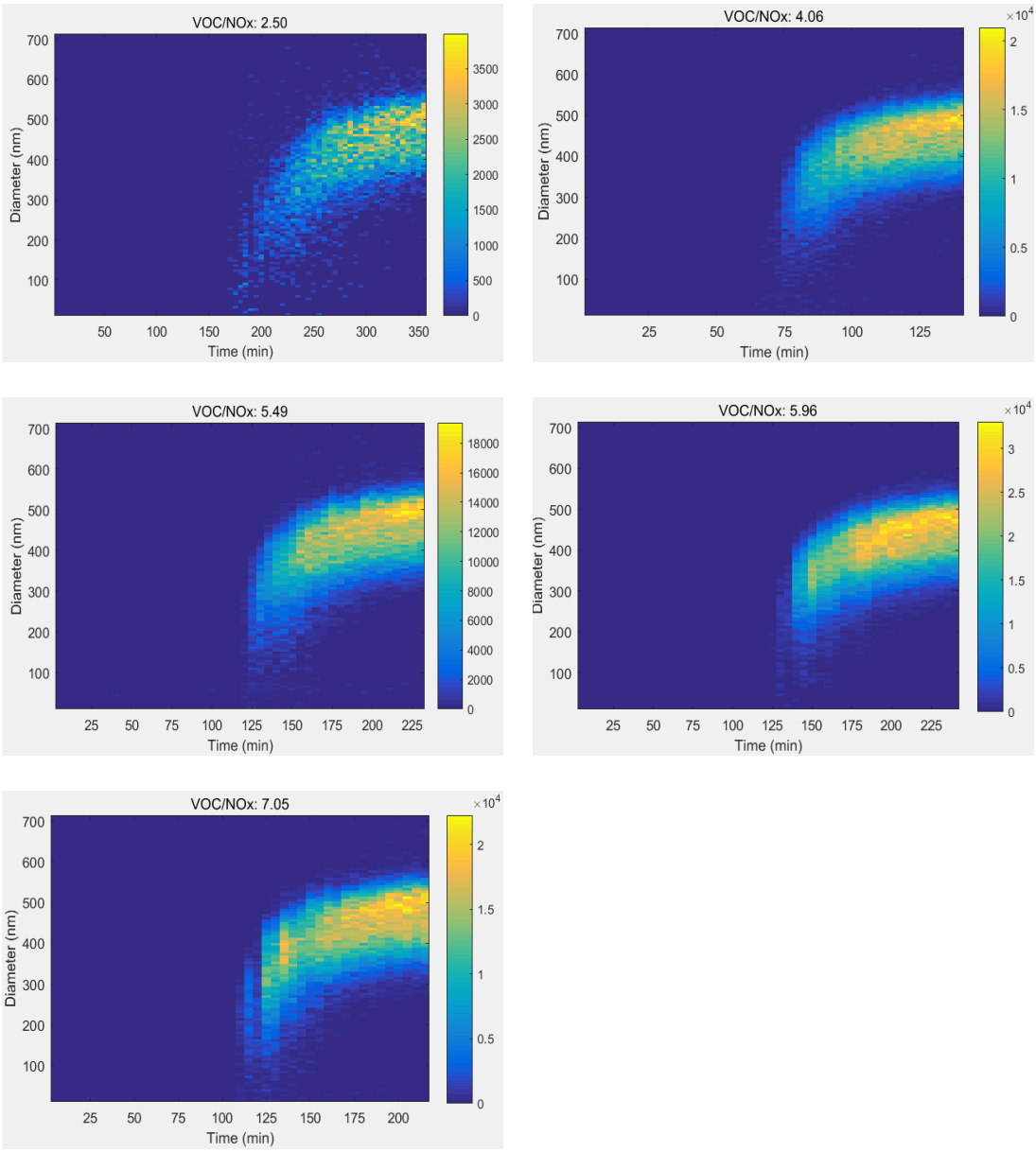

Figure S9. Nanoparticle distribution from 124TMB photooxidation varied with time at different VOC/NO_x ratio (the initial concentrations of NO_x were in the range of 164.4 to 170.3 ppb).

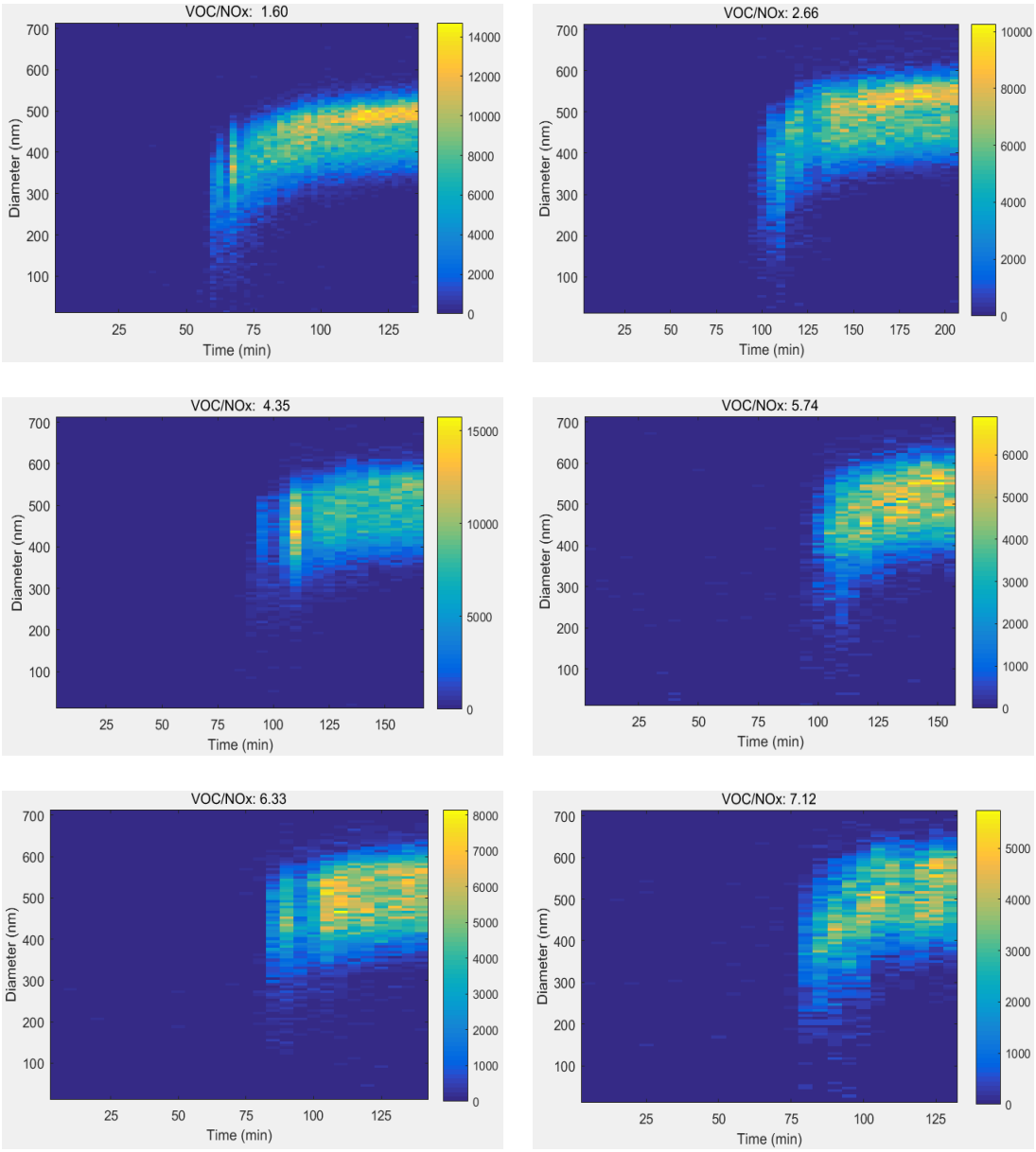

Figure S10. Nanoparticle distribution from 135TMB photooxidation varied with time at different VOC/NO_x ratio (the initial concentrations of NO_x were in the range of 157.4 to 169.7 ppb).

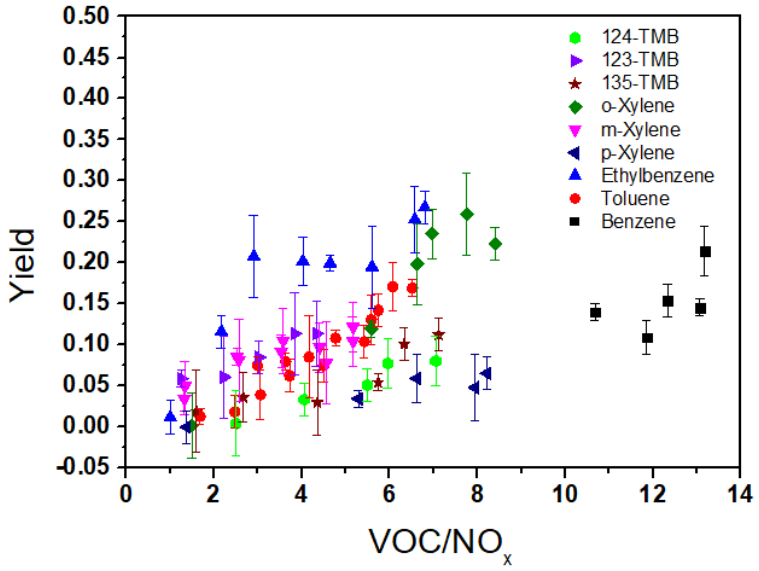

Figure S11. The yield of SOA generated by photochemical oxidation of AHs varies with VOC/NO_x ratio.

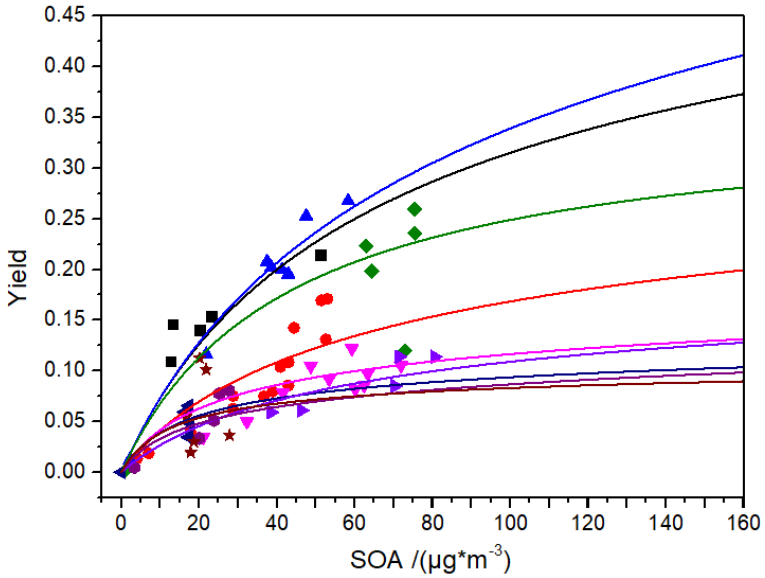

Figure S12. The variation trend of SOA yield generated by photochemical oxidation of different AHs (square: benzene; circle: toluene; upper triangle: ethylbenzene; lower triangle: m-xylene; diamond: o-xylene; left triangle: p-xylene; right triangle: 123TMB； hexagon: 124TMB; pentacle: 135TMB)

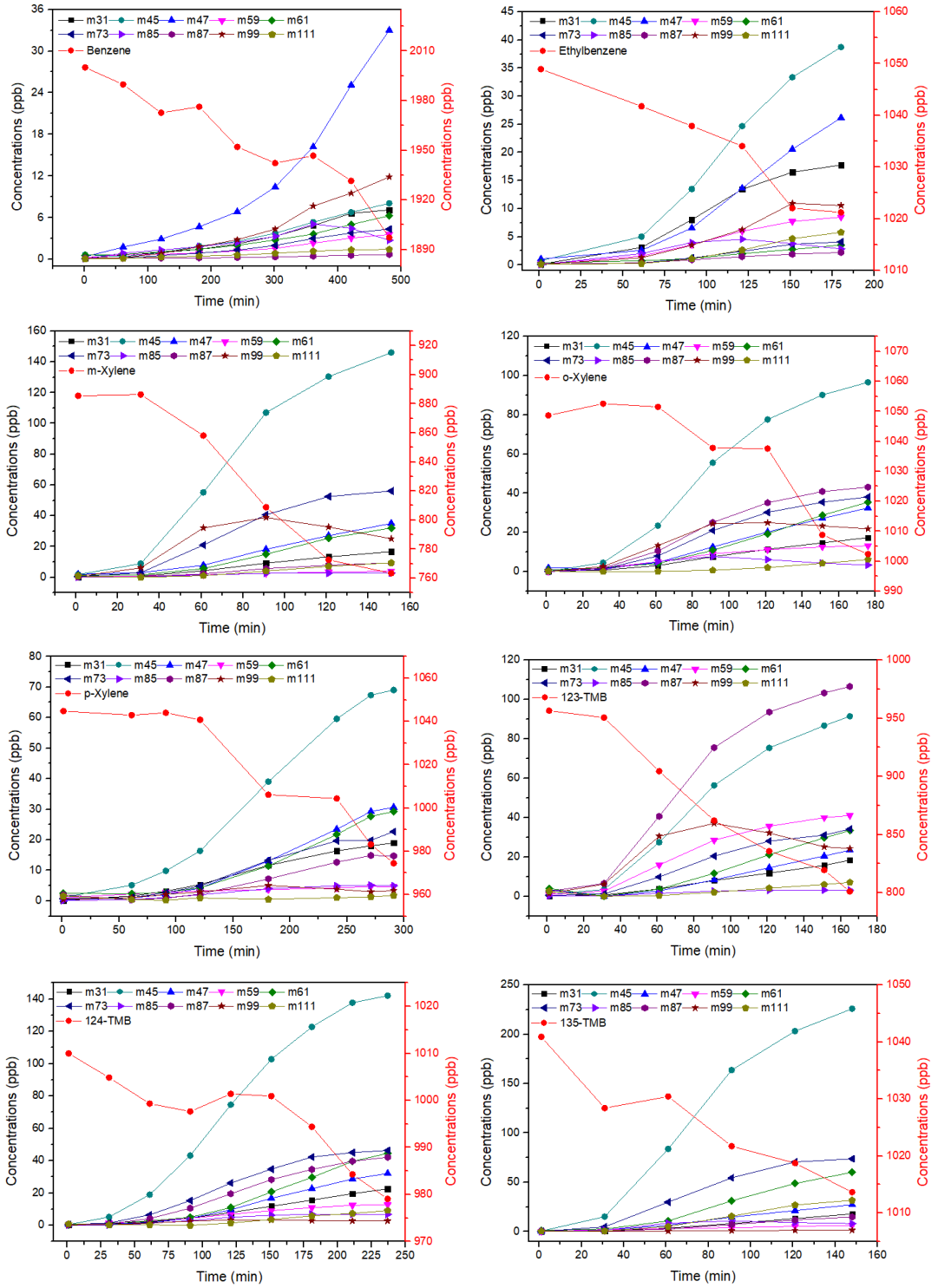

Figure S13. The concentration variation of produced intermediates from photochemical oxidation of different AHs.

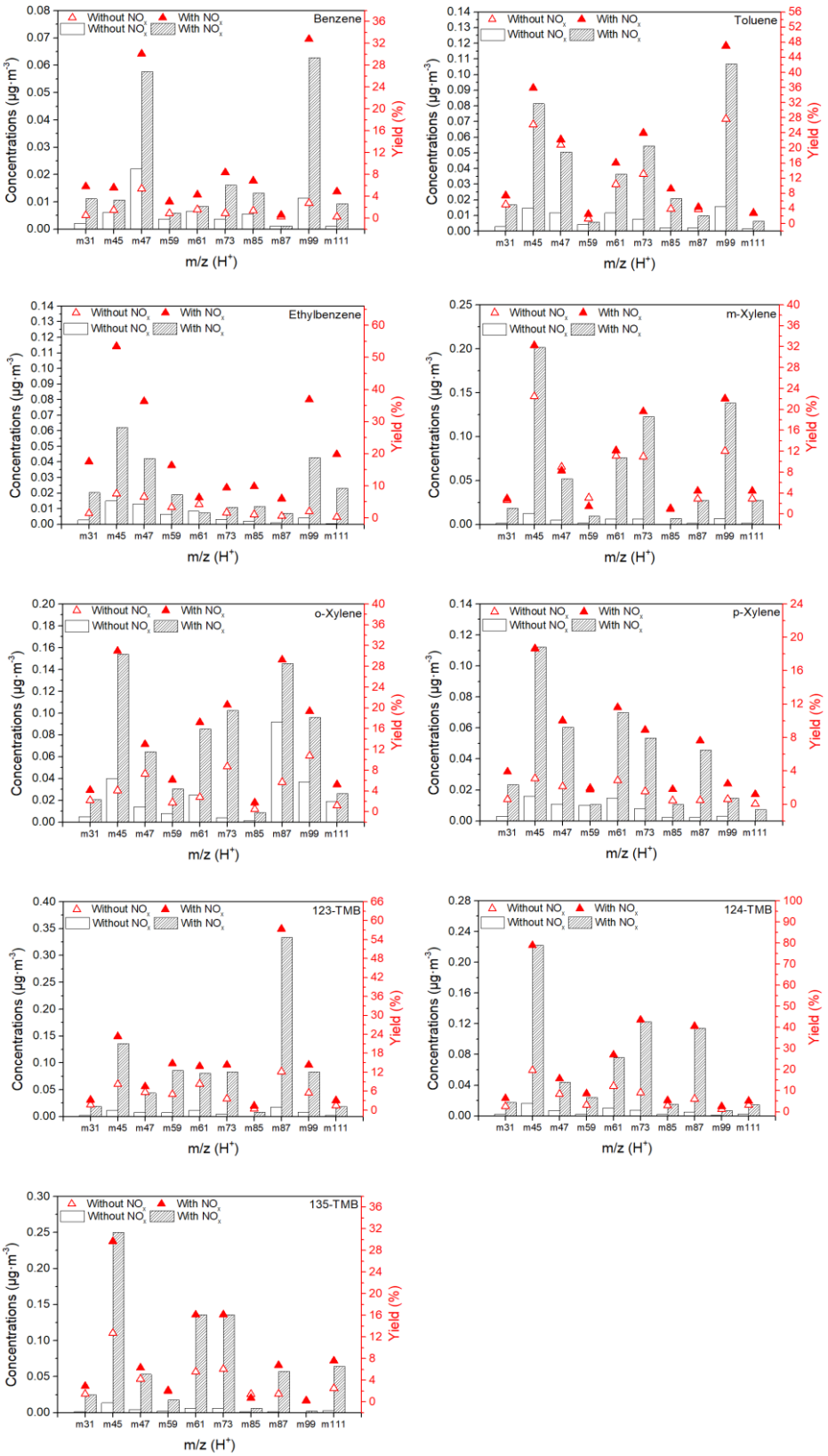

Figure S14. Concentration comparison of produced intermediates from photochemical oxidation of different AHs with or without NO_x.

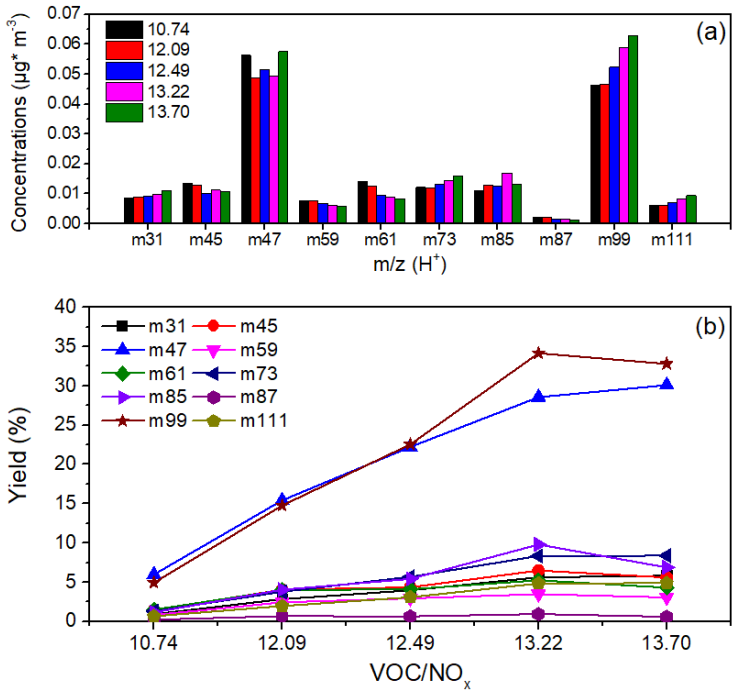

Figure S15. The (a) concentration and (b) yield of products in the gas phase generated by the photochemical oxidation of benzene changed with the trend of VOC/NO_x ratio.

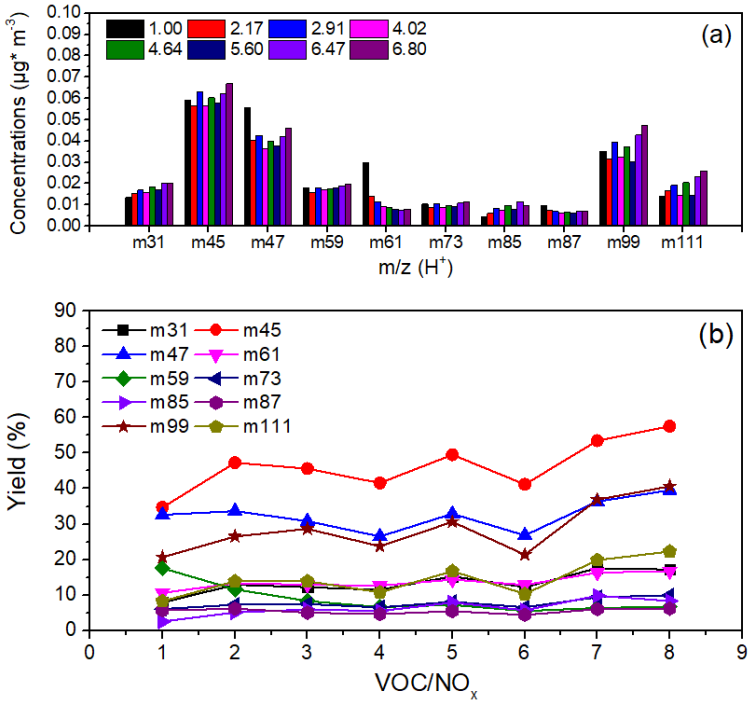

Figure S16. The (a) concentration and (b) yield of products in the gas phase generated by the photochemical oxidation of ethylbenzene changed with the trend of VOC/NO_x ratio.

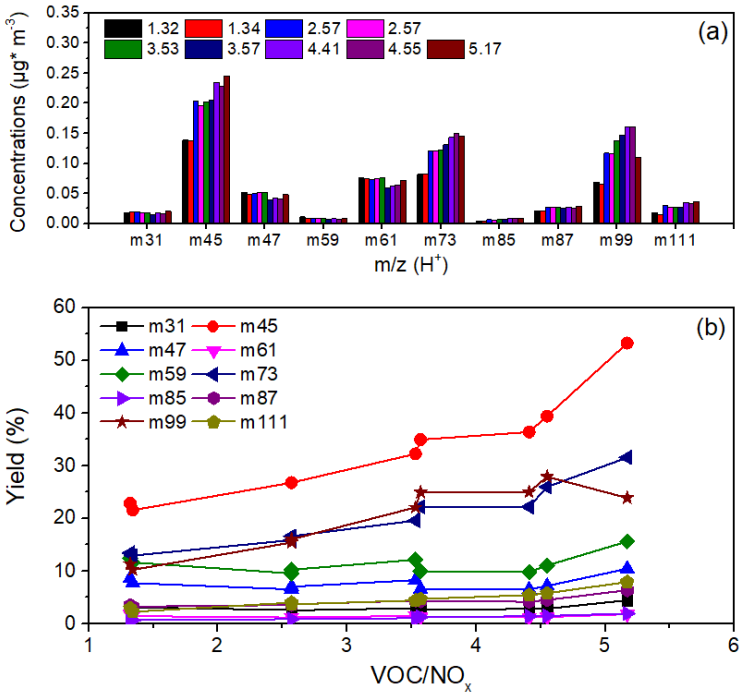

Figure S17. The (a) concentration and (b) yield of products in the gas phase generated by the photochemical oxidation of m-xylene changed with the trend of VOC/NO_x ratio.

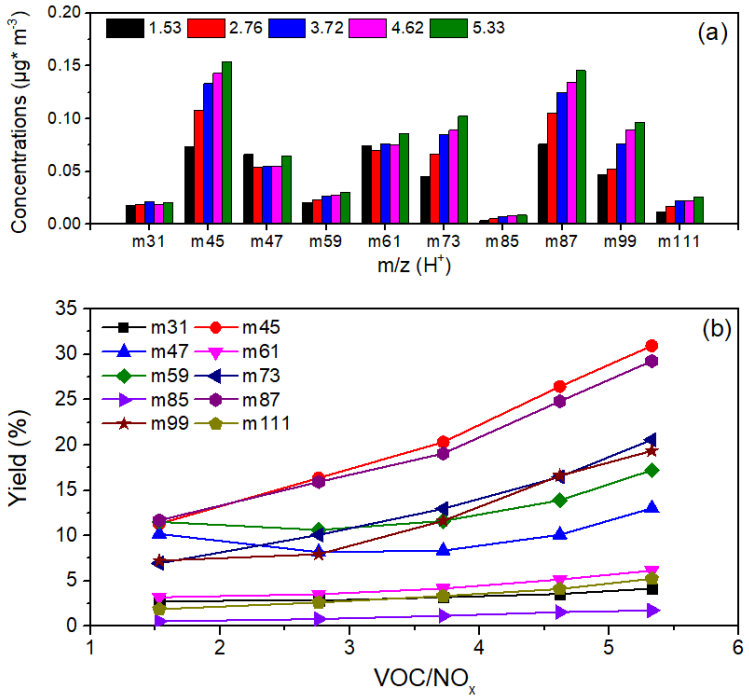

Figure S18. The (a) concentration and (b) yield of products in the gas phase generated by the photochemical oxidation of o-xylene changed with the trend of VOC/NO_x ratio.

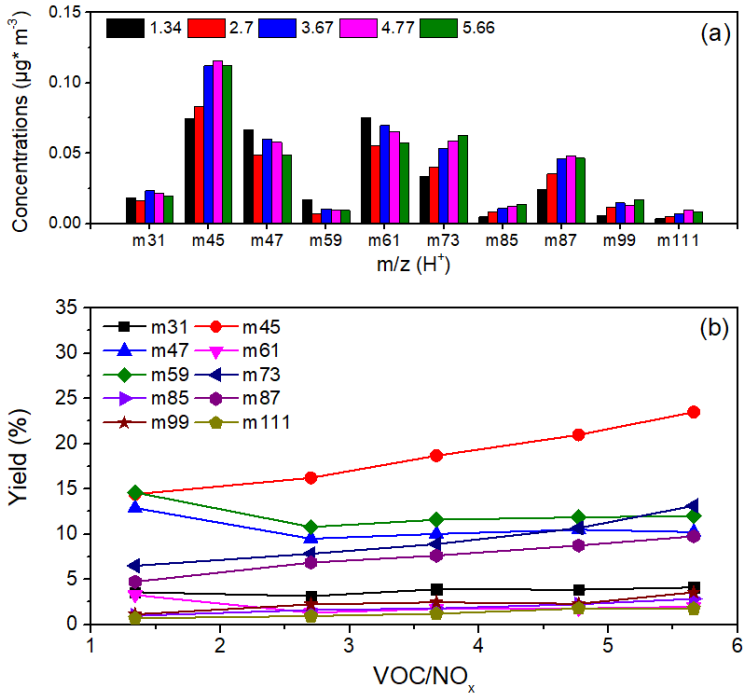

Figure S19. The (a) concentration and (b) yield of products in the gas phase generated by the photochemical oxidation of p-xylene changed with the trend of VOC/NO_x ratio.

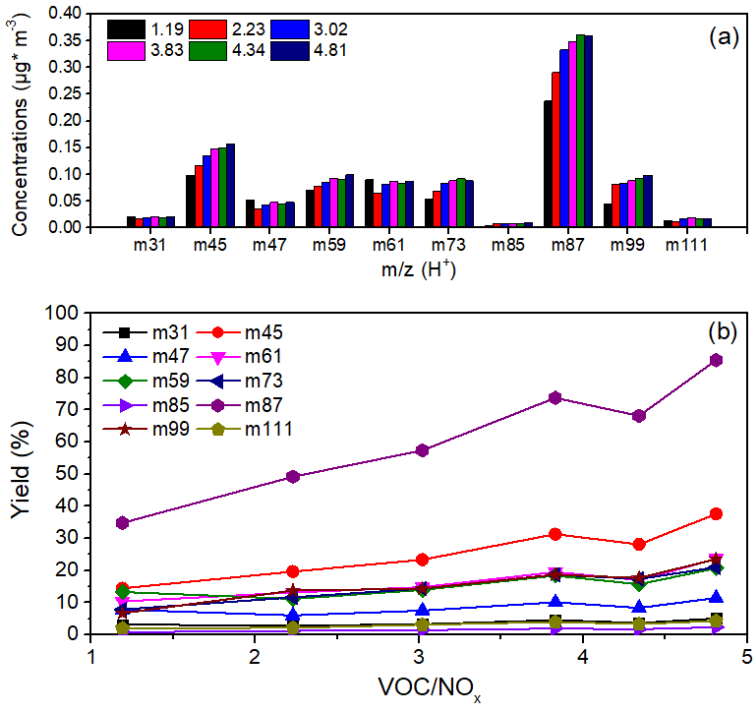

Figure S20. The (a) concentration and (b) yield of products in the gas phase generated by the photochemicaloxidation of 123TMB changed with the trend of VOC/NO_x ratio.

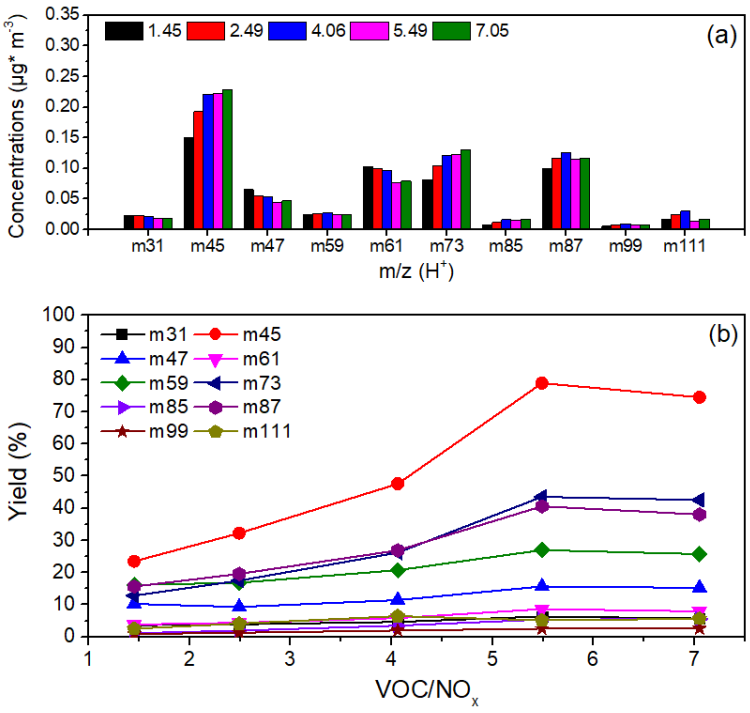

Figure S21. The (a) concentration and (b) yield of products in the gas phase generated by the photochemical oxidation of 124TMB changed with the trend of VOC/NO_x ratio.

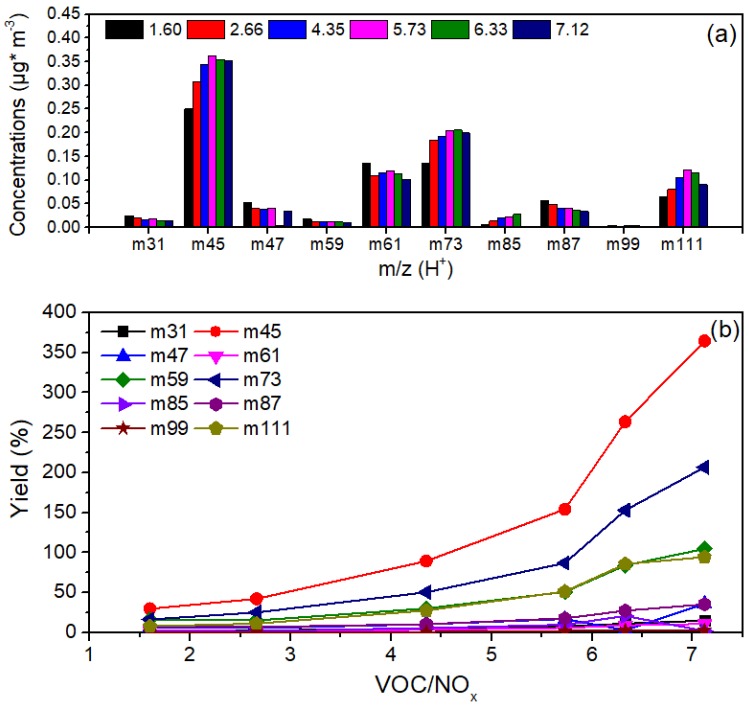

Figure S22. The (a) concentration and (b) yield of products in the gas phase generated by the photochemical oxidation of 135TMB changed with the trend of VOC/NO_x ratio.

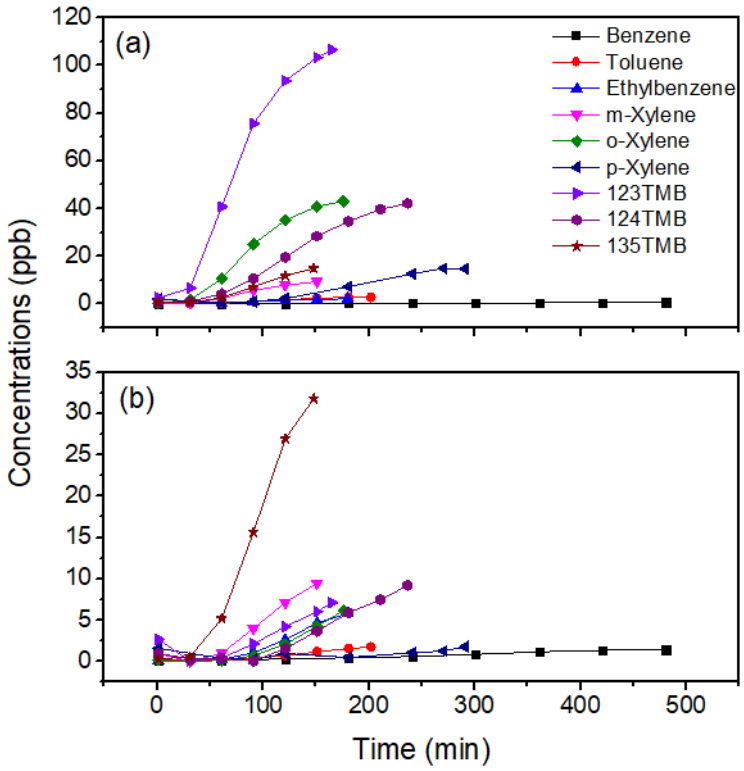

Figure S23. The concentration variation of (a) m87 and (b) m111 formed from different AH photochemical oxidation in the presence of NO_x.

Reference

(1) Odum, J. R.; Hoffmann, T.; Bowman, F.; Collins, D.; C, F. R.; Seinfeld, J. H. Gas/Particle Partitioning and Secondary Organic Aerosol Yields. *Environ Sci Technol* **1996**, *30*, 2580-2585; DOI:

(2) Li, L.; Tang, P.; Nakao, S.; Chen, C. L.; Cocker Iii, D. R. Role of methyl group number on SOA formation from monocyclic aromatic hydrocarbons photooxidation under low-NOx conditions. *Atmospheric Chemistry and Physics* **2016**, *16* (4), 2255-2272; DOI: 10.5194/acp-16-2255-2016.

(3) Borrás, E.; Tortajada-Genaro, L. A. Secondary organic aerosol formation from the photo-oxidation of benzene. *Atmospheric Environment* **2012**, *47*, 154-163; DOI: 10.1016/j.atmosenv.2011.11.020.

(4) Sato, K.; Takami, A.; Isozaki, T.; Hikida, T.; Shimono, A.; Imamura, T. Mass spectrometric study of secondary organic aerosol formed from the photo-oxidation of aromatic hydrocarbons. *Atmospheric Environment* **2010**, *44* (8), 1080-1087; DOI: 10.1016/j.atmosenv.2009.12.013.